Downloaded 07/04/17 to 134.153.188.68. Redistribution subject to SEG license or copyright; see Terms of Use at http://library.seg.org/

Visibility Analysis using Reverse Time Wave Sensitivity for Time-Lapse Target-Oriented Imaging

Andrey H. Shabelansky, Alison Malcolm, and Mike Fehler, Earth Resources Laboratory, Massachusetts Institute of Technology*

SUMMARY

Identifying the relationship between surface seismic data and a particular region in the earth, referred to as visibility analysis, is important because it facilitates the optimization of the quality and speed of the imaging and monitoring processes. This study presents a data-driven approach that estimates a visibility relationship by propagating the recorded seismic data backward in time through the entire medium and coupling it with the region of interest in the subsurface. The region of interest is defined by a specific time-lapse perturbation in geophysical parameters. We show that by back-propagating in time only a limited number of shot records, a reliable visibility relationship can be established for target-oriented imaging of changes in a particular region in the subsurface. The established visibility relationship implies that in a subsequent time-lapse survey, only data corresponding to the visible shot records need to be collected, reducing the costs of the time-lapse acquisitions.

INTRODUCTION

Time-lapse seismic imaging is a method used for monitoring and identifying changes within a reservoir. With these data, it is often only the changes and not the underlying structure that is of interest. In order to efficiently resolve these regions without using an entire data set, one needs to know what data collected on the surface (or in the wells) contributes most to reconstructing an image of these regions. Many studies (Xu and Jin., 2005; Denli and Huang, 2008, 2010; Symes, 2010; Jin. and Xu, 2010) address this problem; however, all of these studies are based on forward modeling a considerable number of shots covering an entire seismic acquisition. We show that by propagating only a relatively small number of shot records backward in time and coupling each time step with the region of interest in the subsurface, we can estimate the visibility relationship between the source locations on the surface (or in the wells) and the region of interest. The visibility relationship is estimated from the sensitivity wavefield, which is calculated by taking the derivative of the wave equation with respect to a geophysical parameter, as described for illumination analysis in Denli and Huang (2008, 2010). Instead of forward propagating a point source, as in Denli and Huang (2008, 2010), we reformulate the algorithm in a data-driven approach, using the recorded seismic data and the principle of reciprocity. This formulation makes the visibility analysis, first, source sensitive for a given set of receivers as opposed to Denli and Huang (2008, 2010), who estimate the sensitivity of receivers for a given source. Second, the estimated visibility relationship indicates which shot records need to be collected in a subsequent time-lapse acquisition, reducing the costs of the time-lapse acquisitions for target-oriented imaging. We refer to the proposed algorithm as reverse time wave sensitivity (RTWS).

In this paper, we outline the underlying theory of the method and test it with two synthetic models. The first model is a simple one-layer model that illustrates the directivity of the source and its relationship with the geometry of the perturbed region. The second model is the Marmousi model (Versteeg and Grau, 1991) with which we show how only a few source locations chosen by the RTWS reliably images the region of interest using reverse time migration (Baysal et al., 1983). Although RTWS can be used in the same manner for full-waveform inversion, this is out of the scope of this paper and it will be discussed elsewhere.

REVERSE TIME WAVE SENSITIVITY

To establish the relationship between the seismic data recorded on the surface and the region of interest inside the earth, we use the principle of time-reversability stating that when the recorded shot gather is propagated backward in time with correct velocity and density models its energy will fully collapse into a single point at the initial position of the source. If the medium is perturbed for the back-propagation, then the back-propagated wavefield will no longer focus entirely at its initial source position and instead some energy will arrive at other positions. In order to use the back-propagated energy due only to the perturbation, we design an algorithm in which the wavefield generated by the perturbation is separated from the total wavefield at each time step of the back-propagation. This algorithm, RTWS, consists of two steps (Figure 1). The first step is the propagation of the seismic shot record backward in time down to the perturbed region in the model (region of interest). We refer to this as the incident wavefield. The second step is the back-propagation of the incident wavefield coupled with the perturbed region, back to the surface. This second wavefield is referred to as the sensitivity wavefield and is the solution of the derivative of the wave equation with respect to velocity, density, or both (Denli and Huang, 2008, 2010). For the sake of simplicity, we use an acoustic 2D model given by the following set of equations:

$$\frac{\partial^2}{\partial t^2}\begin{pmatrix} P_i \\ S_i \end{pmatrix} = \begin{pmatrix} c_1^2\rho_1\nabla\cdot\frac{1}{\rho_1}\nabla & 0 \\ -c_2 V & c_2^2\rho_2\nabla\cdot\frac{1}{\rho_2}\nabla \end{pmatrix}\begin{pmatrix} P_i \\ S_i \end{pmatrix} - \begin{pmatrix} f_i \\ 0 \end{pmatrix}, \tag{1}$$

where time t is propagated backward from the maximum recorded time T toward the recording start ($t = 0$). We denote by $c_j(\mathbf{x})$ and $\rho_j(\mathbf{x})$ the velocities and the densities, where indices $j = 1$ and $j = 2$ correspond to the background and perturbed models, respectively. For the source i, $P_i(\mathbf{x},t)$, $S_i(\mathbf{x},t)$, and $f_i(x,t)$ are, the incident pressure field, the sensitivity field, and the data (i.e. a shot record), respectively. The operator $\nabla = \frac{\partial}{\partial x} + \frac{\partial}{\partial z}$ and $\mathbf{x} = (x,z)$ are the spatial gradient and spatial coordinate consisting of position x and depth z. The perturbation operator $V(\mathbf{x},t)$ is defined as the superposition of pertur-

© 2011 SEG

Downloaded 07/04/17 to 134.153.188.68. Redistribution subject to SEG license or copyright; see Terms of Use at http://library.seg.org/

bations in the velocity and the density models, given as

$$V = \rho_1 \nabla \cdot \frac{\delta\rho}{\rho_1^2} \nabla - \delta\rho \nabla \cdot \frac{1}{\rho_1} \nabla - \frac{2\delta c}{c_1^3} \frac{\partial^2}{\partial t^2} \qquad (2)$$

where the perturbations are defined as

$$\delta c = c_2 - c_1 \qquad \delta\rho = \rho_2 - \rho_1.$$

Note that the perturbations (δc, $\delta\rho$) in the perturbation operator operate not only as sources for the sensitivity field, but also affect its direction of propagation by their geometrical shape.

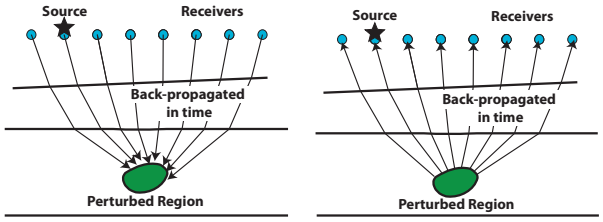

Figure 1: Two steps of RTWS: (a) Propagating the recorded seismic data backward in time from the receiver locations toward the perturbed region, (b) Propagation of the sensitivity wavefield backward in time from the perturbed region toward the surface.

The visibility criteria is defined as the energy of the sensitivity wavefield, calculated for each shot at the grid of possible source locations on the surface at $z = z_0$ (or in the well at $x = x_0$) by

$$E_i(x, z_0) = \int_T^0 S_i^2(x, z = z_0, t)dt. \qquad (3)$$

Since the sensitivity S_i is the wavefield generated from the perturbed region, its high energy as a function of x indicates good visibility between the perturbed region and the source location on the surface, and conversely for low energy.

In general we need to calculate the energy E_i for all shot gathers N_s as

$$E(x, z_0) = \sum_{i=1}^{N_s} E_i(x, z_0). \qquad (4)$$

However, our numerical results indicate that it is sufficient to calculate the energy only for a relatively small number of shots in order to establish a reliable relationship between the region of interest and surface data.

SYNTHETIC TESTS

We test the proposed algorithm with two synthetic models: a one-layer model and data computed in the Marmousi model. In both models we assume, for simplicity, that all receivers are equally distributed on the surface and span the same grid as the sources. All synthetic data and the sensitivity wavefield in Eq. 1 are modeled with a 2D finite-difference solver, using a second order in time staggered-grid pseudo-spectral method with perfectly matched layer (PML) absorbing boundary conditions (Kosloff and Baysal, 1982; Carcione, 1999; Marcinkovich and Olsen, 2003).

Simple One-Layer Model

With this test we illustrate how the geometry of the perturbed region affects the direction of the (backward) propagation of the sensitivity wavefield. To this end, we create a simple one-layer velocity model (Figure 2(a)) through which we generate a shot gather for a source located at $x = 0.36$ km (Figure 2(b)). Using this shot gather as input for RTWS, we test the algorithm with two perturbed velocity models. The first perturbed model contains a single point diffractor (Figure 3(a)) and the second a circular perturbation (Figure 3(b)). Figure 4 shows two snapshots of the reverse sensitivity S_i wavefield at time 1 s, where the back-propagated wavefield P_i is coupled with each of the two perturbed velocity models in Figure 3.

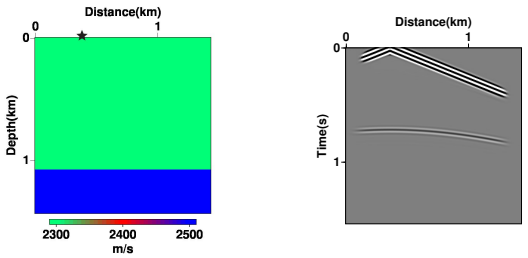

Figure 2: Input data for RTWS analysis: (a) Baseline velocity model. (b) Surface shot record generated at 0.36 km with the baseline velocity model shown in (a).

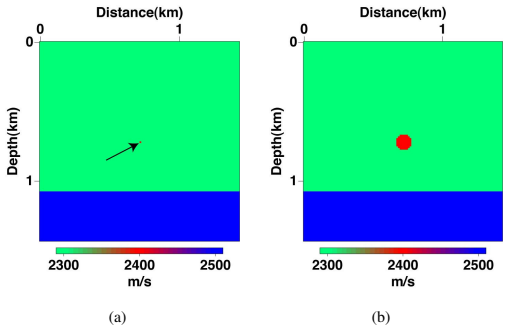

Figure 3: Input perturbed velocity models for RTWS, with perturbations centered at (x, z)=(0.72,0.72) km: (a) Single point perturbation. (b) Circular perturbation.

We observe that for a single point perturbation, the backward-propagated sensitivity wavefront S_i is isotropic (Figure 4(a)). However, for the circular perturbation we observe that sensitivity wavefront S_i has a preferred orientation in back-propagation. This orientation is controlled by the position of source i, generated in this test at 0.36 km on the surface, whose back-propagated shot record defines the direction of the incident P_i and the formed sensitivity S_i wavefields. In Figure 5 we show the en-

© 2011 SEG

Downloaded 07/04/17 to 134.153.188.68. Redistribution subject to SEG license or copyright; see Terms of Use at http://library.seg.org/

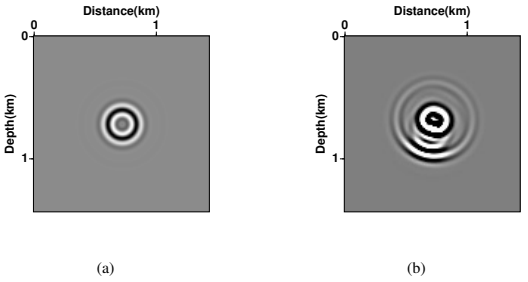

Figure 4: The snapshots of the reverse time sensitivity wavefront at t=1 s, generated with the input shot at 0.36 km and (a) single point perturbation, (b) circular perturbation.

ergy profiles, calculated using Eq. 3, for the sensitivity wavefields at the surface. High sensitivity energy indicates good visibility between the perturbed region in the interior of the earth with the source position on the surface, and conversely for low sensitivity energies. Note that the truncated sensitivity energy at the edges is due to the PML boundary conditions, and does not indicate a zero visibility. The sensitivity energy profiles shown in Figure 5 are generated for a single shot gather. In order to establish a complete relationship, we need to sum the calculated sensitivity energy for each shot gather. In the next section, we show that it is sufficient to calculate the sensitivity energy for a relatively small number of shot gathers.

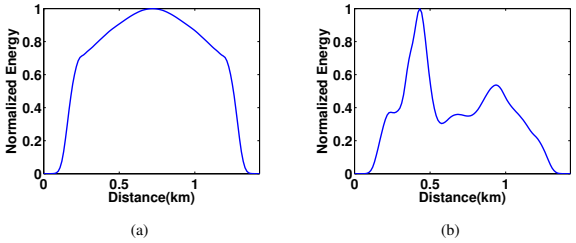

Figure 5: Reverse sensitivity energy profiles recorded on the surface to illustrate the relationship between the recorded seismic shot record and the perturbed region in the earth for (a) point diffractor, (b) circular perturbation.

Sensitivty analysis due to an extended perturbation in the velocity model

To test the algorithm on a more realistic model and to illustrate the importance of sensitivity profiles for target-oriented seismic imaging, we use the Marmousi synthetic model (Figure 6(a)). Since a single point perturbation does not have direction–dependent propagation, we add a general perturbation (marked by a triangle in Figure 6(b)). We calculate the reverse sensitivity energy profiles with shot records for sources at 0.3 km, 1.2 km, and 2.1 km; these profiles are shown in Figure 7.

We observe (in Figure 7) that each energy profile (corresponding to each source location) has its own visibility. Therefore, in theory we need to estimate the reverse sensitivity for each

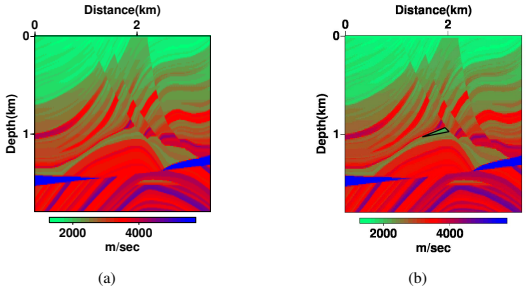

Figure 6: Marmousi velocity model (a) before and (b) after perturbation (marked by the triangle).

surface seismic record. In this test, however, by summing the sensitivity energies from a sparse distribution of sources fully covering the expected range of source locations, we observe that a reliable estimate of the total sensitivity is obtained by summing over only a few sources. Figure 8 shows sensitivity profiles obtained by summing those from different sets of shots. Note that although the profiles are different, the peaks in the profiles are at the same locations within the error of 0.072 km (six grid points) when summing through five and 123 energy profiles. To test this observation, we compute the difference between the summation of a given number of shots spanning the acquisition and the maximum number of shots (N_s=123) used in this test. The formula for this algorithm is given by

$$\varepsilon_k = \sum_{n=1}^{N_x} \left| \sum_{i=1}^{k} E_i(x_n, z_0) - \sum_{i=1}^{N_s} E_i(x_n, z_0) \right| \qquad (5)$$

where N_x is the number of computational grid points at the surface.

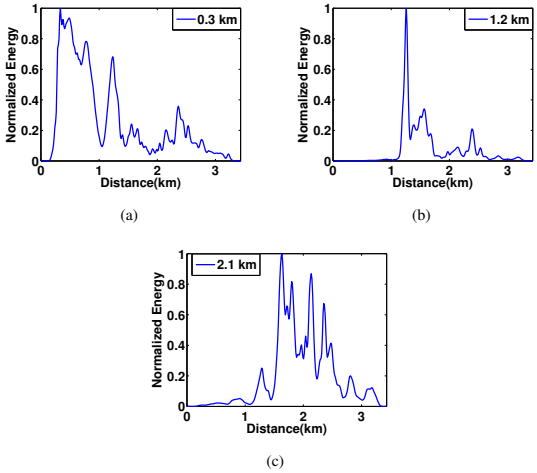

Figure 7: Reverse sensitivity energy profiles generated from shots at positions: (a) 0.3, (b) 1.2, (c) 2.1 km.

Figure 9 shows the normalized ε (given by Eq. 5) as a function of number of shots k used in the calculation. We observe

© 2011 SEG

Downloaded 07/04/17 to 134.153.188.68. Redistribution subject to SEG license or copyright; see Terms of Use at http://library.seg.org/

that we need only a limited number of shots in order to establish a reliable visibility using RTWS. Therefore, by choosing four shot gathers with highest sensitivity energy in Figure 8(a), at 0.768 km, 1.26 km, 1.596 km and 2.484 km, we form a target-oriented image using the reverse time migration (RTM) algorithm. This image of the perturbed region (marked in Figure 6(b)) is shown in Figure 10(a). For comparison, we form three additional images, shown in Figures 10(b), 10(c), and 10(d). The image shown in Figure 10(b) is migrated with four shot gathers that correspond to lowest sensitivity energy at positions 1.08 km, 1.44 km, 2.088 km and 2.76 km, and Figure 10(c) is migrated with shots, arbitrarily and uniformly chosen at positions 1.44 km, 1.68 km, 1.92 km, and 2.16 km. Figure 10(d) is shown as a reference image that is made using all 123 shots with equal spacing of 0.024 km. The image made with the high-visibility shots images the perturbed region, marked by an arrow, better than either the low-visibility or uniformly spaced shots.

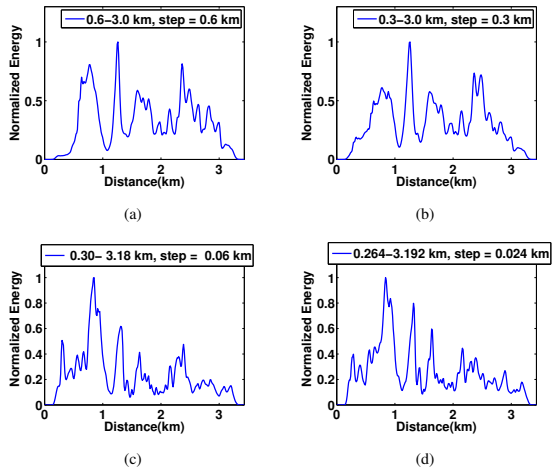

Figure 8: Summed reverse sensitivity energy profiles: (a) the summation of five profiles from 0.6 to 3.0 km with increment of 0.6 km. (b) the summation of ten profiles from 0.3 to 3.0 km with increment of 0.3 km. (c) the summation of 49 profiles from 0.3 to 3.18 km with increment of 0.06 km. (d) the summation of 123 profiles from 0.264 to 3.192 km with increment of 0.024 km.

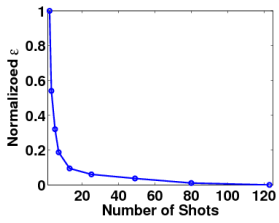

Figure 9: Normalized differential energy according with Eq. 5 calculated for summed energy profiles of equally distributed 2, 3, 5, 7, 13, 25, 49, 79, and 123 shots.

CONCLUSIONS

In this study we presented a data-driven method, the reverse time wave sensitivity, for visibility analysis. This method is based on the propagation of the recorded seismic data backward in time, coupling this back-propagated energy with a known perturbation in a region of interest. We tested this method with two models, a simple one-layer and Marmousi synthetic models. From the first model, we conclude that the geometrical shape of the perturbation affects the back-propagated sensitivity field. From the second model, we conclude that a reliable estimate of the sensitivity energy profile for source positions can be made with relatively few back-propagated shot gathers. The latter conclusion makes the method attractive and efficient for reducing the cost of time-lapse target-oriented imaging and acquisition.

ACKNOWLEDGMENTS

We wish to thank Total inc. for funding this work.

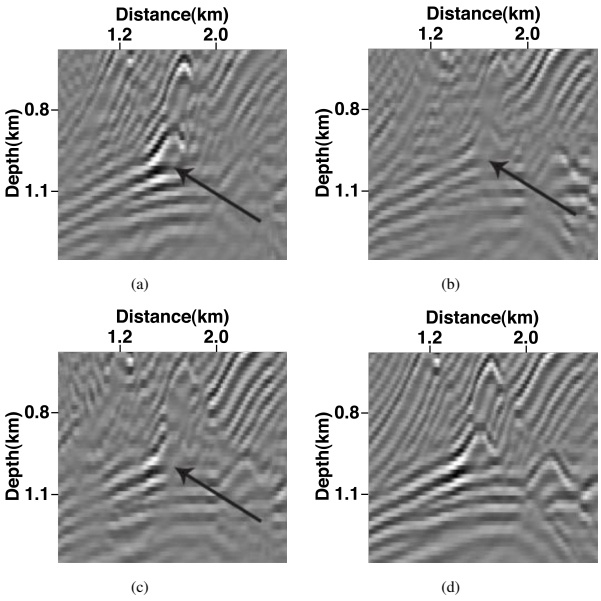

Figure 10: RTM images with four shots migrated with: (a) maximum reverse sensitivity energy (positions 0.768 km, 1.26 km, 1.596 km and 2.484 km). (b) minimum reverse sensitivity energy (positions 1.08 km, 1.44 km, 2.088 km and 2.76 km). (c) arbitrary equally-spaced locations at positions (1.44 km, 1.68 km, 1.92 km and 2.16 km). (d) An image was migrated for reference with all 123 shots with equally-spaced increment of 0.024 km.

© 2011 SEG

Downloaded 07/04/17 to 134.153.188.68. Redistribution subject to SEG license or copyright; see Terms of Use at http://library.seg.org/

EDITED REFERENCES

Note: This reference list is a copy-edited version of the reference list submitted by the author. Reference lists for the 2011 SEG Technical Program Expanded Abstracts have been copy edited so that references provided with the online metadata for each paper will achieve a high degree of linking to cited sources that appear on the Web.

REFERENCES

Baysal, E., D. D. Kosloff, and J. W. C. Sherwood, 1983, Reverse time migration: Geophysics, **48**, 1514–1524, doi:10.1190/1.1441434.

Carcione, J. M., 1999, Staggered mesh for the anisotropic and viscoelastic wave equation: Geophysics, **64**, 1863–1866.

Denli, H., and L. Huang, 2008, Elastic-wave sensitivity analysis for seismic monitoring: 78th Annual International Meeting, SEG, Expanded Abstracts, 30–34.

———, 2010, Elastic-wave sensitivity propagation: Geophysics, **75**, no. 3, T83–T97, doi:10.1190/1.3428403.

Jin, S., and S. Xu, 2010, Visibility analysis for target-oriented reverse time migration and optimizing acquisition parameters: The Leading Edge, **29**, 1372–1377.

Kosloff, D. D., and E. Baysal, 1982, Forward modeling by a Fourier method: Geophysics, **47**, 1402–1412, doi:10.1190/1.1441288.

Marcinkovich, C., and K. Olsen, 2003, On the implementation of perfectly matched layers in a three-dimensional fourth order velocity-stress finite difference scheme: Journal of Geophysical Research, **108**, no. 18, 1–16.

Symes, W., 2010, Source synthesis for waveform inversion: 80th Annual International Meeting, SEG, Expanded Abstracts, 1018–1022.

Versteeg, R., and G. Grau, eds., 1991, The Marmousi experience: Proceedings of the 1990 EAEG workshop on practical aspects of seismic data inversion: EAEG.

Xu, S., and S. Jin, 2005, Can we image beneath salt body? — Target-oriented visibility analysis: 75th Annual International Meeting, SEG, Expanded Abstracts, 1997–2000.

© 2011 SEG